Published in "Dalton Transactions 47(2): 596–607, 2018"
which should be cited to refer to this work.

cis- and *trans*-9,10-di(1*H*-imidazol-1-yl)-anthracene based coordination polymers of Zn^{II} and Cd^{II}: synthesis, crystal structures and luminescence properties†

Serhii I. Vasylevskyi,*[a] Khrystyna Regeta,[b] Albert Ruggi,[a] Stéphane Petoud,[c] Claude Piguet[c] and Katharina M. Fromm*[a]

New functional coordination polymers based on the semi-flexible 9,10-di(1*H*-imidazol-1-yl)-anthracene ligand (**L**) with Zn^{II} and Cd^{II}, namely $\{[Zn(\mu_2\text{-}\mathbf{L})_2](ClO_4)_2{\cdot}m(MeOH){\cdot}n(DCM)\}_n$ (**1**), $\{[Zn(\mu_2\text{-}\mathbf{L})_2](BF_4)_2{\cdot}m(MeOH){\cdot}n(DCM)\}_n$ (**2**), $\{[Zn(\mu_2\text{-}\mathbf{L})_2(p\text{-Tos})_2]{\cdot}m(DCM){\cdot}n(MeOH)\}_n$ (**3**), $\{[Cd(\mu_2\text{-}\mathbf{L})_2(p\text{-Tos})_2]{\cdot}m(DCM)\}_n$ (**4**) $\{[Cd(\mu_2\text{-}\mathbf{L})_2(p\text{-Tos})_2]{\cdot}m(MeOH){\cdot}n(Dioxane)\}_n$ (**5**) and $\{[Zn(\mu_2\text{-}\mathbf{L})_2(CF_3CO_2)_2]{\cdot}2(Dioxane)\}_n$ (**6**), were obtained. Dissolving **L** in polar solvent mixtures MeOH–DCM (4 : 1) or MeOH–dioxane (1 : 1) with Zn^{II} and Cd^{II} salts resulted in the formation of complexes **1**, **2**, and **5** adopting a *cis*-conformation of the imidazole groups with respect to anthracene. In less polar mixtures of solvents such as MeOH–DCM (1 : 4) *trans*-**L** is observed, leading to the coordination polymers **3–4** with Zn^{II} and Cd^{II}. In an intermediate solvent mixture such as MeOH–dioxane (1 : 4), the *cis*- and *trans*-conformation coexist as exemplified in complex **6** with Zn^{II}. In the solid state, complexes **1–5** assemble as supramolecular 2-D coordination polymers with a (***4,4***) topology, while **6** forms a tridimensional porous network with a ***cds*** topology. All compounds reveal strong blue emission in the solid state at room temperature.

Introduction

Functional coordination polymers (CPs) are of great interest not only because of their unique structure topologies, but also because of their diverse applications in MOLED devices,[1] non-linear optics,[2] sensors,[3] fluorescent materials,[4] magnetism,[5] adsorption and separation of gas mixtures[6] as well as in heterogeneous catalysis.[7] The choice of building blocks with desired properties is therefore a key aspect in the chemistry of hybrid organic–inorganic materials to obtain desired properties. This has inspired chemists over the last two decades to develop and investigate new functional CPs.[8,9]

Luminescent CPs based on the anthracene moiety are one of the areas of extensive interest, as these compounds can have applications in different technological fields, *e.g.* triplet–triplet annihilation (TTA),[10] luminescent sensors for hazardous molecules, detection of anions and cations,[11] and bioimaging of biological objects and diagnostic agents.[12] Indeed, anthracene and its derivatives are known to possess attractive luminescence properties including large quantum yields.[13] The incorporation of this chromophoric moiety into a ligand could enhance the luminescence intensity of the latter and confer this property to CPs upon binding with *e.g.* Zn^{II} and Cd^{II}. Imidazole-based groups were those that were widely used over the last decade to produce a broad variety of 2-D and 3-D coordination polymers.[14] We propose here a new approach for the synthesis of highly luminescent, bidentate 9,10-bis-imidazole-anthracene ligand **L** (Chart 1) and its use for the synthesis of luminescent 2-D and 3-D polymeric functional materials upon coordination with Zn^{II} and Cd^{II}. We also show how these CPs can be used in sensing applications for nitro compounds.

Experimental

Materials and methods

All commercially available chemicals were of reagent grade and were used as received without further purification. $Zn(p\text{-Tos})_2{\cdot}n(H_2O)$ and $Cd(p\text{-Tos})_2{\cdot}n(H_2O)$ were prepared from corresponding carbonates of the metal ions.[15] 9,10-Dibromoanthracene was prepared following a literature procedure.[24]

[a]*University of Fribourg, Chemistry Department, Chemin du Musée 9, 1700 Fribourg, Switzerland. E-mail: serhii.vasylevskyi@unifr.ch, katharina.fromm@unifr.ch*
[b]*Universidade Nova de Lisboa, Departamento de Física, 2829-516 Caparica, Portugal*
[c]*University of Geneva, Department of Inorganic and Analytical Chemistry, 30 Quai Ernest-Ansermet, 1211 Geneva 4, Switzerland*

† Electronic supplementary information (ESI) available. CCDC 1549435–1549436, 1549445–1549446, 1549456 and 1549459.

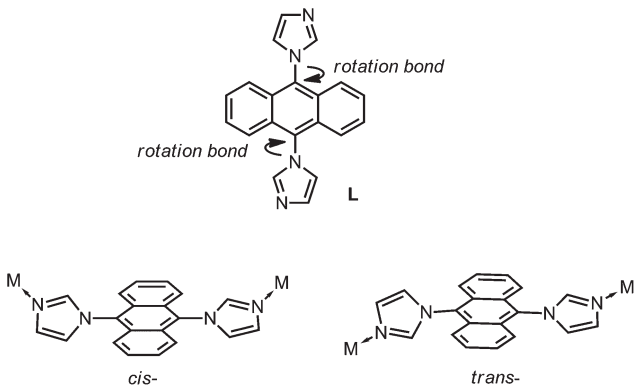

Chart 1 Ligand **L**: 9,10-di(1-*H*-imidazol-1-yl)-anthracene and its two possible *cis*- and *trans*-conformations in coordination polymers.

^{1}H-NMR and ^{13}C-NMR spectra were recorded on a 400 MHz and a Bruker 100 MHz spectrometer at room temperature with $CDCl_3$ and d^6-DMSO as solvents and tetramethylsilane (TMS) as the internal standard. Mass spectra were recorded on a Bruker–ION Trap MS. Fluorescence spectra were measured on an Edinburgh Instruments FS5 Spectrofluorometer and on a modified Horiba Scientific Fluorolog. Lifetime measurements were conducted using a LifeSpec II (EPL pulsed diode laser, Edinburg). Absorption spectra were collected on a PerkinElmer UV/VIS/NIR Lambda 900 (190–1100 nm) spectrophotometer. IR absorption spectra were recorded on a PerkinElmer FT-IR spectrometer Frontier 4000–400 cm^{-1}. Single crystal diffraction data were obtained from a STOE-IPDS II (single crystal diffractometer λ-Mo, Kα radiation, λ = 0.71073 Å), and the structures were solved and refined using the SHELXT-97 software package.[16]

Synthetic procedures

Synthesis of the ligand (L). 9,10-Di(1-*H*-imidazol-1-yl)-anthracene was synthesized by using a modified literature procedure by Lee *et al.*[24] 9,10-Dibromoanthracene (9.00 g, 26.78 mmol), imidazole (7.28 g, 107.14 mmol) and sodium hydroxide (4.28 g, 107.14 mmol) were placed into a 100 mL flask under magnetic stirring. Dry DMF was added and the mixture was heated to 120 °C for 3 h. The advancement of the reaction was monitored by TLC (eluent: THF–Hex = 1 : 5). After the completion of the reaction, the mixture was cooled to rt. The greyish precipitate was filtered, washed with excess amounts of water to attain neutral pH, and finally with 150 mL of hexane to obtain a pale white precipitate, which was dried under reduced pressure for 24 h (7.2 g, 86%).

^{1}H-NMR: δ 7.83 (2H, d, J = 0.89 Hz, imidazole), 7.58–7.52 (8H, m, anthracene), 7.50 (2H, s, imidazole), 7.34 (2H, d, J = 0.89 Hz, imidazole) (Fig. S1 and 2†).

^{13}C-NMR: δ 139.61 (2C$_{tert.}$, anthracene), 139.58 (2C–H, imidazole), 130.14 (2C–H, imidazole), 128.14 (4C–H, anthracene), 122.80 (2C–H, imidazole), 122.78 (4C–H, anthracene) (Fig. S3†).

HRMS: Calc. 310.12; obtained: $[M + H]^+$ 311.1288 (Fig. S5†).

IR (KBr, cm^{-1}): 3092m, 1487s, 1439m, 1413s, 1327m, 1109m, 1081s, 1028s, 907s, 803s, 768s, 655s, 633m, 604w, 420m.

Synthesis of the complexes 1–6

{[Zn(μ$_2$-L)$_2$](ClO$_4$)$_2$·*m*(MeOH)·*n*(DCM)}$_n$ (1). A mixture of $Zn(ClO_4)_2{\cdot}6H_2O$ (18.6 mg, 0.05 mmol) in 4 mL of MeOH was layered over a DCM solution (1 mL) of **L** (15 mg, 0.05 mmol). Colourless prism-like crystals were collected after 3 days. Yield based on **L**: ∼68%.

Anal. calc. for ($C_{43}H_{36}Cl_6N_8O_9Zn$): C, 47.52%; H, 3.34%; Cl, 19.57%; N, 10.31%; O, 13.25%; Zn, 6.02%.

Found: C, 47.40%; H, 3.33%; N, 10.57%. Corresponds to the formula unit [Zn(**L**)$_2$](ClO$_4$)$_2$·1(MeOH)·2(DCM).‡

IR (KBr, cm^{-1}): 3457w, 3130w, 1622m, 1513s, 1443m, 1412s, 1323m, 1255m, 1224w, 1113s, 1084s, 954s, 911m, 845m, 769s, 741s, 687m, 658s, 621s, 434s, 416s.

{[Zn(μ$_2$-L)$_2$](BF$_4$)$_2$·*m*(MeOH)·*n*(DCM)}$_n$ (2). **2** was obtained by using a similar procedure to the one used for complex **1**, except for using $Zn(BF_4)_2{\cdot}nH_2O$ instead of $Zn(ClO_4)_2{\cdot}6H_2O$. Yield based on ligand **L**: ∼60%.

Anal. calc. for ($C_{43}H_{36}B_2Cl_4F_8N_8OZn$): C, 48.65%; H, 3.42%; B, 2.04%; Cl, 13.36%; F, 14.32%; N, 10.56%; O, 1.51%; Zn, 6.16%.

Found: C, 48.16%; H, 3.51%; N, 10.37%. Corresponds to the formula unit [Zn(**L**)$_2$](BF$_4$)$_2$·1(MeOH)·2(DCM).§

IR (KBr, cm^{-1}): 3457w, 3144w, 1624m, 1514s, 1443m, 1414s, 1324m, 1285m, 1256m, 1226m, 1113s, 1087s, 954s, 912s, 850s, 769s, 742s, 688m, 659s, 604m, 521m, 433s, 416s.

{[Zn(μ$_2$-L)$_2$(*p*-Tos)$_2$]·*m*(DCM)·*n*(MeOH)}$_n$ (3). **3** was synthesized using a similar method to that of **2** with the exception of Zn(*p*-Tos)$_2$·nH_2O replacing $Zn(BF_4)_2{\cdot}nH_2O$ and using a solvent ratio of 1 : 4 MeOH–DCM. Colourless block-like crystals were obtained, yield based on ligand **L**: ∼52%.

Anal. calc. for $C_{56}H_{50}N_8O_8S_2Zn$: C, 61.56%; H, 4.61%; N, 10.25%; O, 11,71%; S, 5.87%; Zn, 5.98%.

Found: C, 61.25%; H, 4.38%; N, 10.41%; S, 5.97% for [Zn(**L**)$_2$(*p*-Tos)$_2$] 2(MeOH).‡

IR (KBr, cm^{-1}): 3664w, 3390w, 3095w, 1625 m, 1500 m, 1440w, 1416 m, 1325w, 1220 m, 1170s, 1118s, 1081s, 1033s, 1010s, 934 m, 912 m, 820 m, 769s, 679s, 658s, 605w, 566s, 417 m, 405w.

{[Cd(μ$_2$-L)$_2$(*p*-Tos)$_2$]·*m*(DCM)}$_n$ (4). **4** was synthesized using a similar method to that of **3**, except for using Cd(*p*-Tos)$_2$·nH_2O instead of Zn(*p*-Tos)$_2$·nH_2O. Yield based on ligand **L**: ∼79%.

Anal. calc. for $C_{55}H_{44}CdCl_2N_8O_6S_2$: C, 56.93%; H, 3.82%; Cd, 9.69%; Cl, 6.11%; N, 9.66%; O, 8.27%; S, 5.53%.

Found: C, 57.66%; H, 3.75%; N, 9.72%; S, 5.39% for [Cd(**L**)$_2$(*p*-Tos)$_2$]·1(DCM).‡

IR (KBr, cm^{-1}): 3664w, 3450w, 3095w, 1624w, 1495m, 1440w, 1416m, 1323w, 1284w, 1235s, 1222s, 1165s, 1120s,

‡ The formulae of complexes **1–6** were found from elemental analyses and might slightly deviate from those calculated for the crystal structures determined by single crystal X-Ray diffraction, due to the presence of volatile solvents in the structures *e.g.* DCM, MeOH, and dioxane.

§ Solid state UV-Vis, PL, QY and lifetime measurements for the obtained complexes were measured in air; stable composition was revealed by elemental analysis.

1082s, 1034s, 1010s, 931m, 912m, 868w, 814w, 770s, 746m, 682s, 667s, 616w, 605w, 566s, 416m, 405w.

{[Cd(μ$_2$-L)$_2$(*p*-Tos)$_2$]·*m*(MeOH)·*n*(Dioxane)}$_n$ (5). **5** was synthesized using a similar method to that of **4**, except for using 1 : 1 of MeOH–dioxane solution. Yield based on the ligand **L**: ~83%.

Anal. calc. for $C_{60}H_{58}CdN_8O_{10}S_2$: C, 58.88%; H, 4.38%; Cd, 8.89%; N, 8.86%, O, 13.92%; S, 5.07%.

Found: C, 58.82%; H, 4.65%; N, 9.23%; S, 5.08% for [Cd(**L**)$_2$(*p*-Tos)$_2$]·2(MeOH)·(Dioxane).‡

IR (KBr, cm^{-1}): 3144w, 3118w, 3089m, 2957w, 2911w, 2883w, 2842m, 1625m, 1601w, 1494s, 1441s, 1416s, 1321m,

Table 1 Crystal data and structure refinement parameters for complexes **1–6**

Compound	**1**	**2**	**3**	**4**	**5**	**6**
Formula	$C_{42}H_{36}Cl_2N_8O_{10}Zn$	$C_{42}H_{36}B_2F_8N_8O_2Zn$	$C_{58}H_{54}Cl_4N_8O_8S_2Zn$	$C_{56}H_{46}CdCl_4N_8O_6S_2$	$C_{64}H_{66}CdN_8O_{12}S_2$	$C_{52}H_{44}F_6N_8O_8Zn$
$D_{calc.}$/g cm^{-3}	1.324	1.300	1.397	1.467	1.423	1.456
Formula weight	949.08	923.80	1262.38	1245.34	1315.76	1088.32
T/K	200(2)	200(2)	200(2)	250(2)	200	200
Crystal system	Monoclinic	Monoclinic	Triclinic	Monoclinic	Monoclinic	Monoclinic
Space group	$C2/c$	$C2/c$	$P\bar{1}$	$P2_1/n$	$P2_1/n$	$P2_1/c$
a/Å	22.1784(12)	22.2863(8)	11.7749(19)	9.2922(9)	10.6432(3)	13.6068(5)
b/Å	13.3509(7)	13.1735(6)	12.2678(19)	22.5731(13)	13.3880(4)	18.0054(5)
c/Å	16.1723(9)	16.2124(6)	12.1740(19)	13.4673(12)	21.5624(6)	20.3919(7)
α/°	90	90	111.157(12)	90	90	90
β/°	96.174(4)	97.265(3)	93.629(13)	93.281(7)	91.374(2)	96.256(3)
γ/°	90	90	110.389(12)	90	90	90
V/Å^3	4760.9(4)	4721.6(3)	1500.9(4)	2820.2(4)	3071.57(15)	4966.2(3)
Q_{min}/°	1.783	1.799	1.837	1.763	1.791	1.513
Q_{max}/°	25.119	25.082	25.172	25.192	25.168	25.344
R_{int}	0.0990	0.0734	0.1103	0.1080	0.0342	Twin
GooF	1.010	1.046	1.035	0.804	1.071	1.036
wR_2 [b] (all data)	0.1427	0.1164	0.1386	0.1355	0.1533	0.1664
wR_2	0.1309	0.1111	0.1312	0.1171	0.1458	0.1493
R_1 (all data)	0.0876	0.0602	0.0622	0.1248	0.0692	0.1085
R_1 [a]	0.0564	0.0463	0.0518	0.0495	0.0583	0.0838

[a] $R_1 = \sum||F_o| - |F_c||/\sum|F_o|$. [b] $Rw = [\sum[w(F_o^2 - F_c^2)^2]/\sum w(F_o^2)^2]^{1/2}$.

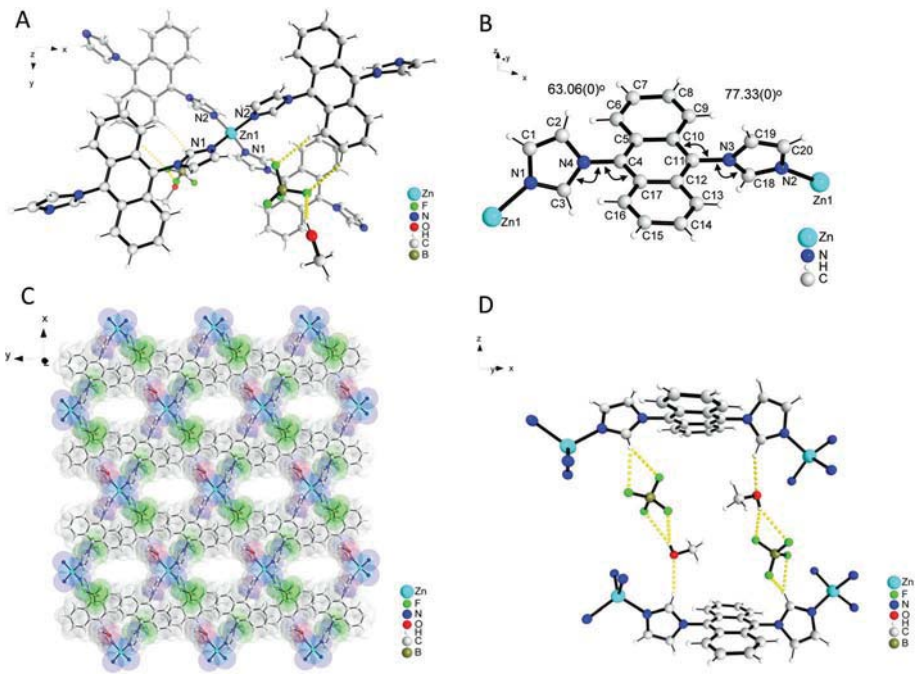

Fig. 1 Crystal structures of compounds **1** and **2**: (A) Representation of the coordination unit of the compound {[Zn(μ$_2$-**L**)$_2$](BF$_4$)$_2$·2(MeOH)·2(DCM)}$_n$; (B) *cis*-conformation of the ligand **L** in the structures **1** and **2**, revealing different torsion angles of imidazole planes with respect to anthracene with 76.02(1)° and 63.09(1)°; (C) self-assembly of **L** and Zn(ClO$_4$)$_2$ or Zn(BF$_4$)$_2$ with the formation of a 2D polymer with a crystal topology of the lattices ***4,4***; (D) presence of weak interactions with anions and guest molecules of methanol and imidazole groups from **L** in structure **1** and **2**.

1239s, 1222s, 1166s, 1111s, 1078s, 931s, 912m, 821m, 810m, 770s, 682s, 662s, 567s, 548v–s, 416s.

{[Zn(μ$_2$-L)$_2$(CF$_3$CO$_2$)$_2$]·2(Dioxane)}$_n$ (6). **6** was synthesized using a procedure similar to that of **5**, except for using Zn(CF$_3$CO$_2$)$_2$·n(H$_2$O) instead of Cd(p-Tos)$_2$·n(H$_2$O) and the 1 : 4 mixture of MeOH–dioxane. Yield based on the **L**: ~95%.

Anal. calc. for $C_{52}H_{44}F_6N_8O_8Zn$: C, 57.38%; H, 4.05%; F, 10.47%; N, 10.29%; O, 11.76%; Zn, 6.00%.

Found: C, 57.22%; H, 4.09%; N, 10.26% for formula unit: [Zn(**L**)$_2$(CF$_3$CO$_2$)$_2$]·2(Dioxane).‡

IR (KBr, cm^{-1}): 3135m, 2957m, 2912w, 2888w, 2853m, 2752w, 2690w, 1688v–s, 1695m, 1595m, 1526m, 1509s, 1442m, 1426m, 1415s, 1329m, 1323m, 1252s, 1150–1081v–s, 1034m, 951m, 912m, 888m, 870s, 844s, 795m, 777s, 655s, 612s, 520m, 499m, 417m.

Crystallography

X-Ray single-crystal diffraction data for **1–6** were collected on a STOE IPDS II at 200–250 K with Mo Kα radiation (λ = 0.71073 Å). The program X-Area[17] was used for the integration of the diffraction profiles. All the structures were solved by direct methods using the SHELXT program of the SHELX package and refined by using full-matrix least-squares methods with SHELXL (integration absorption corrections were applied using the X-Red program).[17] Metal atoms in each complex were located from the E-maps and other non-hydrogen atoms were located in successive difference Fourier syntheses and refined with anisotropic thermal parameters on F^2. The hydrogen atoms of the ligands were generated theoretically on the specific atoms and refined isotropically with fixed thermal factors. The hydrogen atoms of the solvent molecules were located from Fourier maps and refined with isotropic temperature factors. Further details of the structural analysis are summarized in Table 1.

Structures can be found by the following CCDC reference numbers 1549435, 1549436, 1549446, 1549445, 1549459, and 1549456.†

Results and discussion

Synthesis details and general characterization

9,10-Di(1-*H*-imidazol-1-yl)-anthracene was synthesized by using a modified procedure relevant to a classical Ullmann amination coupling,[15b] which usually applies for aromatic halogen derivatives. In our case, we used sodium hydroxide in DMF for the deprotonation of the imidazole groups which react with 9,10-dibromoanthracene to obtain the bis-substituted ligand **L** in high yield. Further reaction with Zn^{II} or Cd^{II} salts resulted in the formation of complexes **1–6**, which were characterized by elemental analyses, IR absorption spectroscopy and single crystal X-ray diffraction as well as with respect to their optical properties. Although all the reactions of metal salts with the **L** ligand were carried out under similar experimental conditions using a molar ratio of 1 : 1, we observed that the resulting 2-D and 3-D coordination polymers **1–6** systematically contained a ratio of M : **L** = 1 : 2.

The infrared spectra of **1–6** all exhibit the characteristic absorption bands for **L**, yet with a slight shift due to coordination. The absorption bands at 1118 cm^{-1} and 1098 cm^{-1} indicate the presence of ClO$_4^-$ and BF$_4^-$ anions in **1** and **2**, respectively. In **3–5**, the absorption bands at 1165 cm^{-1} and 1127 cm^{-1} are characteristic of the coordinated tosylate ions.[18] In compound **6**, additional bands assigned to the stretching vibration of C–F bonds at 1415 cm^{-1}, C═O at 1703 cm^{-1} and C–O at 1197 cm^{-1} confirm the presence of CF$_3$CO$_2^-$ anions.

Crystal structure description

The isostructural compounds **{[Zn(μ$_2$-L)$_2$](ClO$_4$)$_2$·2(MeOH)·2(DCM)}$_n$ (1)** and **{[Zn(μ$_2$-L)$_2$](BF$_4$)$_2$·2(MeOH)·2(DCM)}$_n$ (2)** crystallize in the *monoclinic* space group, $C2/c$. The single crystal X-ray diffraction analysis revealed that, in **1** and **2**, the Zn^{II} ion adopts a pseudo-tetrahedral environment, which is constituted by four nitrogens belonging to four bidentate *N*,*N*-bridging ligand molecules (Fig. 1a). All bond lengths around the Zn^{II} ion are within the normal range (Table 2). The bond angles

Table 2 Selected bond distances (Å) and angles (°) for complexes **1–6**

1			
Zn(1)–N(1)	1.983(3)	N(1)–Zn(1)–N(1)$^{\#1}$	112.62(2)
Zn(1)–N(1)$^{\#1}$	1.983(3)	N(1)$^{\#1}$–Zn(1)–N(2)$^{\#2}$	107.11(1)
Zn(1)–N(2)$^{\#2}$	1.993(3)	N(1)–Zn(1)–N(2)$^{\#2}$	109.50(1)
Zn(1)–N(2)$^{\#3}$	1.993(3)	N(1)–Zn(1)–N(2)$^{\#3}$	107.11(1)
		N(2)$^{\#3}$–Zn(1)–N(2)$^{\#2}$	111.04(2)
2			
Zn(1)–N(1)	1.989(2)	N(1)–Zn(1)–N(1)$^{\#1}$	111.49(1)
Zn(1)–N(1)$^{\#1}$	1.989(2)	N(1)$^{\#1}$–Zn(1)–N(2)$^{\#2}$	107.04(9)
Zn(1)–N(2)$^{\#2}$	1.999(2)	N(1)–Zn(1)–N(2)$^{\#2}$	109.80(9)
Zn(1)–N(2)$^{\#3}$	1.999(2)	N(1)–Zn(1)–N(2)$^{\#3}$	107.04(9)
		N(2)$^{\#3}$–Zn(1)–N(2)$^{\#2}$	111.72(1)
3			
Zn(1)–N(1)	2.129(2)	N(1)–Zn(1)–O(1)	90.20(9)
Zn(1)–N(3)$^{\#1}$	2.141(2)	N(1)$^{\#1}$–Zn(1)–O(1)	89.80(9)
Zn(1)–O(1)	2.142(2)	N(3)$^{\#1}$–Zn(1)–O(1)	89.26(1)
N(1)–Zn(1)–N(3)$^{\#1}$	90.42(9)	N(3)–Zn(1)–O(1)	90.74(1)
N(1)$^{\#1}$–Zn(1)–N(3)$^{\#1}$	89.58(9)	N(1)–Zn(1)–O(1)$^{\#1}$	89.80(9)
4			
Cd(1)–O(1)$^{\#1}$	2.312(4)	N(1)$^{\#1}$–Cd(1)–O(1)	87.2(2)
Cd(1)–N(1)$^{\#1}$	2.303(6)	N(1)$^{\#1}$–Cd(1)–O(1)$^{\#1}$	92.8(2)
Cd(1)–N(4)$^{\#2}$	2.328(6)	N(1)–Cd(1)–N(4)$^{\#3}$	95.34(2)
Cd(1)–N(4)$^{\#3}$	2.328(6)	N(1)–Cd(1)–N(4)$^{\#2}$	84.66(2)
O(1)–Cd(1)–N(4)$^{\#2}$	85.5(2)	N(1)$^{\#1}$–Cd(1)–N(4)$^{\#3}$	84.67(2)
O(1)$^{\#1}$–Cd(1)–N(4)$^{\#2}$	94.5(2)		
5			
Cd(1)–O(1)$^{\#1}$	2.289(3)	N(1)–Cd(1)–N(2)$^{\#2}$	90.40(12)
Cd(1)–N(1)	2.318(3)	O(1)–Cd(1)–N(1)	87.94(13)
Cd(1)–N(2)$^{\#2}$	2.335(3)	O(1)–Cd(1)–N(2)$^{\#2}$	91.78(14)
N(1)$^{\#1}$–Cd(1)–N(2)$^{\#2}$	89.60(12)	O(1)$^{\#1}$–Cd(1)–N(2)$^{\#2}$	88.22(14)
6			
Zn(1)–N(1)	2.110(4)	N(1)–Zn(1)–O(1)	84.52(15)
Zn(1)–N(2)	2.155(4)	N(1)–Zn(1)–O(2)	96.08(15)
Zn(1)–N(3)	2.105(4)	N(1)–Zn(1)–N(2)	88.33(15)
Zn(1)–N(4)$^{\#1}$	2.165(4)	N(1)–Zn(1)–N(4)$^{\#1}$	92.23(15)
Zn(1)–O(1)	2.166(3)	N(2)–Zn(1)–O(1)	90.61(16)
Zn(1)–O(2)	2.200(4)	N(2)–Zn(1)–O(2)	87.98(15)

Symmetry codes: **1–2** #1: $1 - X$, $+Y$, $3/2 - Z$; #2: $3/2 - X$, $-1/2 + Y$, $3/2 - Z$; #3: $-1/2 + X$, $-1/2 + Y$, $+Z$. **3** #1: $1 - X$, $1 - Y$, $1 - Z$; #2: $1 - X$, $-Y$, $-Z$; #3: $-X$, $-Y$, $1 - Z$. **4** #1: $2 - X$, $1 - Y$, $2 - Z$; #2: $-1/2 + X$, $3/2 - Y$, $1/2 + Z$; #3: $5/2 - X$, $-1/2 + Y$, $3/2 - Z$. **5** #1: $-x$, $1 - y$, $-z$; #2: $1/2 - x$, $-1/2 + y$, $1/2 - z$; **6** #1: $1/2 + x$, $1/2 - y$, $-1/2 + z$.

around the Zn^{II} ions significantly deviate from an ideal tetrahedral angle of 109.5°, but are still in the range of typical pseudo-tetrahedral coordination[19] (N–Zn–N = 107.04(9) to 112.62(2)°) (Fig. S7, S15†). The N-donor atoms which belong to the two terminal imidazole functional groups located on one ligand molecule adopt a *cis*-conformation and have their planes tilted by 63.09(1)° and 76.02(1)° for **1** and 63.06(1)° and 77.33(1)° for **2** with respect to the plane of the anthracene moiety (Fig. 1b, S10, S14†). Each Zn^{II} atom is interconnected through four **L** to four different Zn^{II} ions thus leading to 2-D layers with a (***4***,***4***)-topology within the *ab*-plane (Fig. 1c, S8†). The tetrahedral ClO_4^- and BF_4^- anions are located above and below the 2-D network. A short contact distance of 2.333(3) Å for **1** and 2.316(1) Å for **2** connects the methanol molecules with one proton of imidazole groups (Fig. 1d), while protons from methanol molecules are also involved in short contact distances with the *Td* anions ClO_4^-(**1**): O(5)–H(5)···O(4) = 2.301(3) Å or BF_4^- (**2**): O(1)–H(1A)···F(2) = 2.240(2) Å (Fig. 1d, S6, S13†). The anions themselves also have short contacts with protons from imidazole groups from a neighbour 2-D lattice at distances of 2.388(2) Å and 2.334(2) Å (2) (Fig. 1d, S6, S14†). Thus, through weak interactions, topological identical nets are bound at distances of 8.5 Å from each other to form the 3-D supramolecular structure of **1** and **2** (Fig. 1c, S11†). Due to disordered solvent molecules within the 2D lattice, the contents of the pores were squeezed,[28] and the total residual electron density was assigned to two molecules of MeOH and four molecules of DCM.

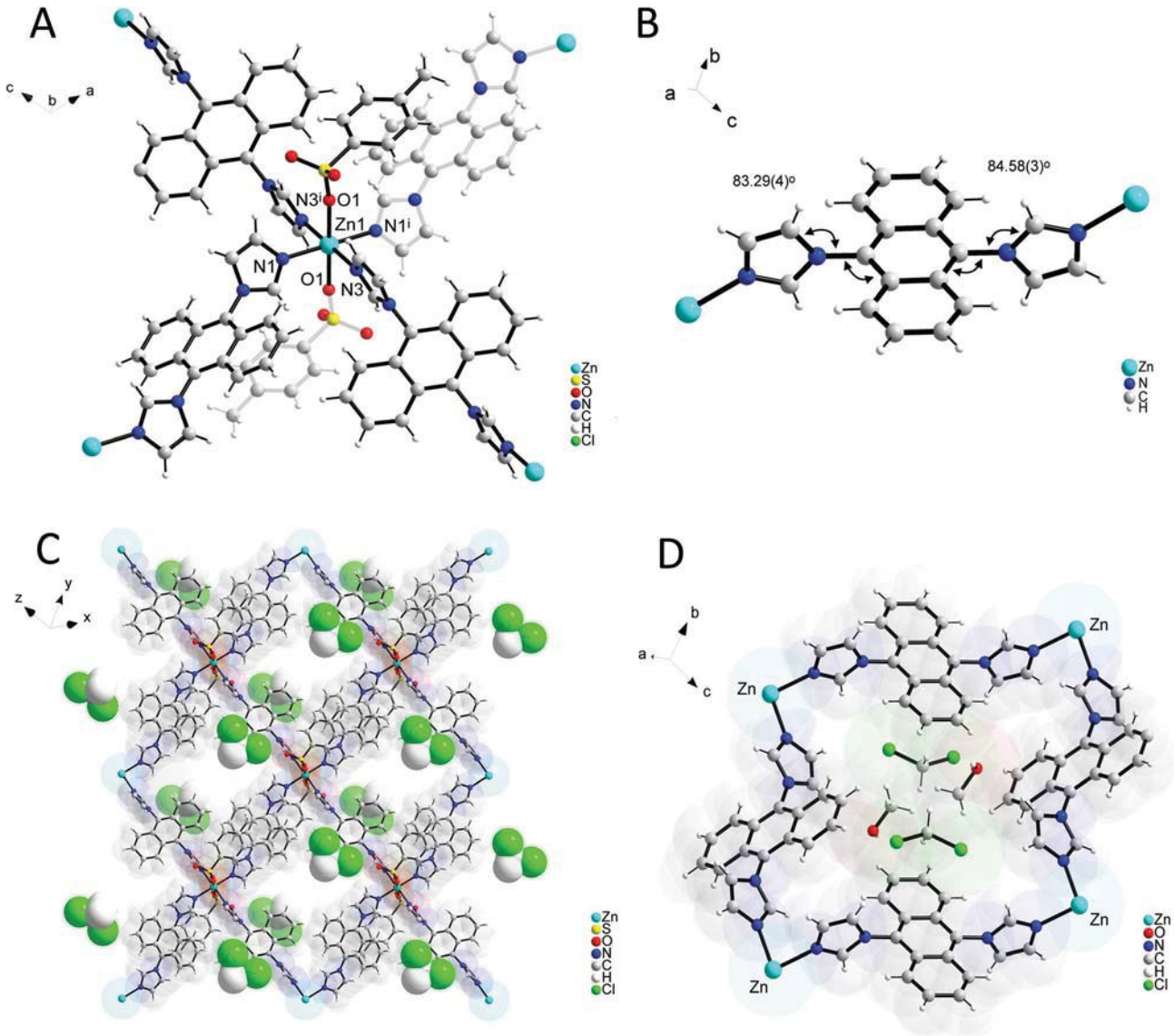

Fig. 2 Crystal structure of compound **3**: (A) representation of the coordination unit of $\{[Zn(\mu_2\text{-}L)_2(p\text{-}Tos)_2]\cdot 2(DCM)\cdot 2(MeOH)\}_n$; (B) revealing *trans*-conformation of **L** with torsion angles of imidazole with respect to anthracene planes 84.58(3)° and 83.29(4)°; (C) assembly of $Zn(p\text{-}Tos)_2$ with **L** → formation of 2-D net with topology (*4,4*), guest molecules are located above or below the lattice plane; (D) representing the rhombohedral grid of Zn where molecules of DCM and methanol are trapped.

{[Zn(μ$_2$-L)$_2$(*p*-Tos)$_2$]·2(DCM)·2(MeOH)}$_n$ (3). Compound **3** crystallizes in the *triclinic* space group $P\bar{1}$. **3** shows rhombic grids extending infinitely along the *ab*-plane, where the nodes of the grid contain Zn^{II} ions, which are connected through linkers of **L**. In contrast to **1** and **2**, each Zn(II) ion in **3** adopts a slightly distorted octahedral coordination geometry formed by four N-donor atoms Zn(1)–N(1) = 2.129(2) Å, Zn(1)–N(3) = 2.141(2) Å from four molecules of **L** in equatorial positions and by two oxygen atoms Zn(1)–O(1) = 2.142(2) Å from two tosylate anions occupying the axial positions (Table 2). The coordination angles vary from N(1)–Zn(1)–O(1) = 90.20(9)° to 89.80(9)° (Fig. 2a and Table 2). The ligand molecules now adopt a *trans*-conformation of the imidazole groups with respect to the anthracene moiety (Fig. 2b).

Fig. 2c shows that each Zn^{II} is connected to four neighbouring Zn^{II} atoms by four **L** ligands, forming $[Zn(\mu_2\text{-}L)_4]^{2+}$ coordination units and Zn_4L_4 "squares". The Zn···Zn diagonals in such a square amount to 17.484 Å and 21.301 Å (Fig. S20†). These squares are assembled within the *ab*-plane to give a (***4,4***)-net-topology. The guest methanol and dichloromethane (DCM) molecules show an interesting feature: the methanol molecules are connected to the oxygen atoms from tosylate anions at a distance of O(3)–H(4a) = 2.108(2) Å with an "acceptor–donor–acceptor" angle of 162.18(3)° (Fig. 2d, S21†), corresponding to weak hydrogen bonding. DCM molecules display a short halogen contact to another oxygen from the tosylate anion at a distance of Cl(1)–O(3) = 3.036(2) Å (Fig. S21†). A second chlorine atom takes part in the contact of Cl(2)–H(19) = 2.864(1) Å with a proton from the anthracene group, while at the same time DCM protons are involved in short contacts with oxygen atoms from tosylate anions of another layer at a distance of H(29a)–O(2) = 2.579(1) Å and O(3) = 2.707(1) Å (Fig. S22†). As a result of such interactions of guest molecules, which are trapped between identical (***4,4***)-nets, a 3-D supra-

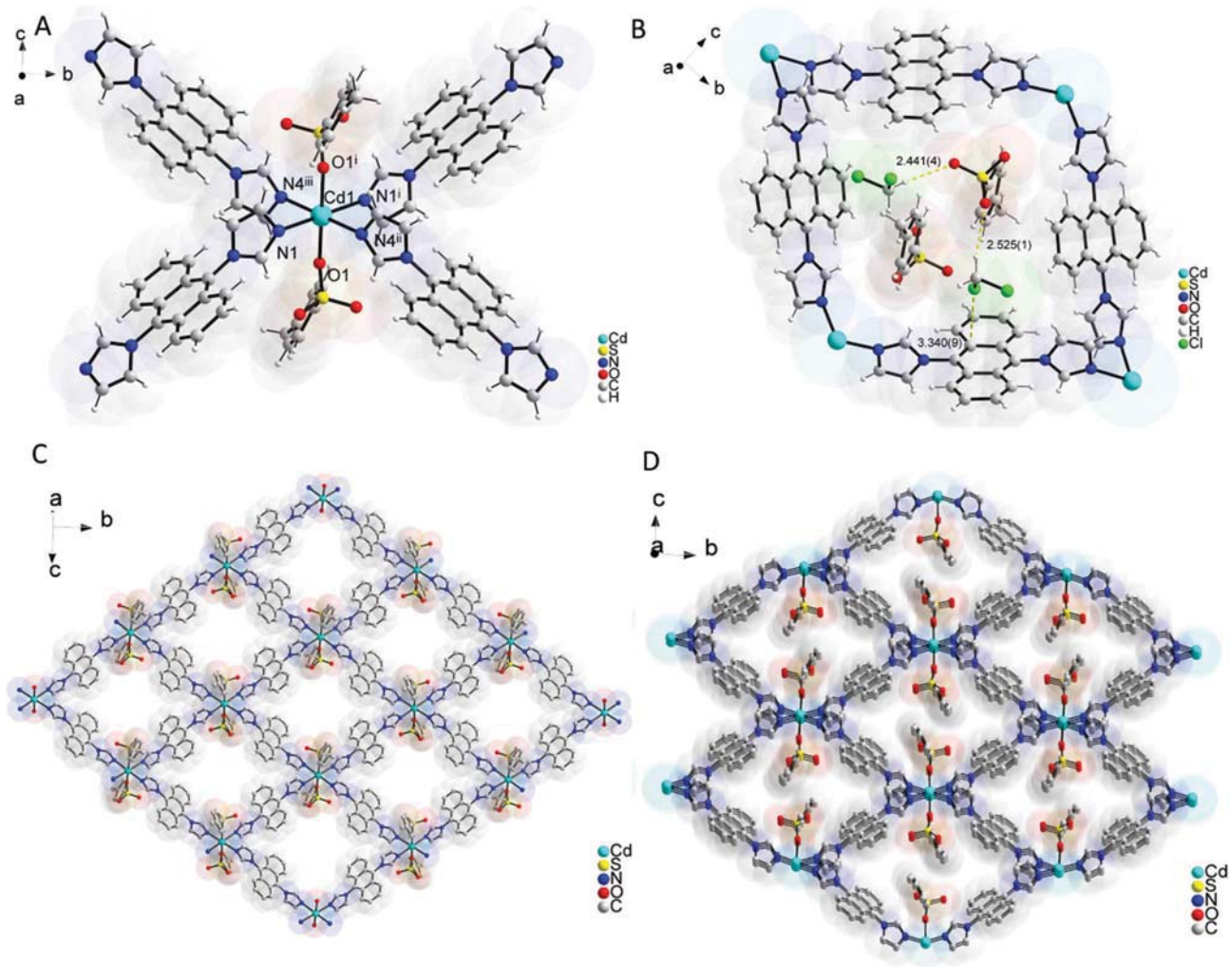

Fig. 3 Crystal structure of compound **4**: (A) representation of the coordination unit of {[Cd(μ$_2$-L)$_2$(*p*-Tos)$_2$]·2(DCM)}$_n$; (B) formation of the 2-D coordination polymer net of Cd^{II} with topology (*4,4*); (C) self-assembly of Cd^{II} and ligand **L** with formation of the rhombical grid of Cd, by π-Cl interactions of the guests : DCM molecules with anthracene moieties in distance 3.340(9) Å and short contact of DCM with oxygen from tosylate anions [O···H 2.525(1) Å]; (D) connection of 2-D nets through weak interaction leads to the formation of a 3-D polymer with 1D channels where molecules of DCM and tosylate anions are lodged.

molecular polymer of Zn^{II} is formed, which has encapsulated methanol and dichloromethane molecules in between the lattice layers (Fig. S24 and S25†).

{[Cd(μ$_2$-L)$_2$(*p*-Tos)$_2$]·2(DCM)}$_n$ (4). The self-assembly of Cd(OTs)$_2$ and **L** in methanol–DCM solution gives compound **4**, which crystallizes in the *monoclinic* space group, $P2_1/n$. The Cd^{II} ions adopt pseudo-octahedral coordination geometries similar to those found around Zn^{II} ions in compound **3**. Each Cd^{II} is coordinated by four N-atoms belonging to four bridging *trans*-ligand molecules (Fig. 3a, S30†), with distances of Cd(1)–N(1) = 2.303(6) Å and Cd(1)–N(4) = 2.328(6) Å (Fig. 3a, Table 2). The axial positions are occupied by oxygen atoms from tosylate anions with a distance of Cd(1)–O(1) = 2.312(4) Å (Fig. 3a). The angles around the Cd^{II} ion are between N(1)–Cd(1)–O(1) = 87.2(2)° and N(4)–Cd(1)–O(1) = 94.5(2)° and deviate more strongly from the ideal octahedral geometry compared to compound **3**. As for Zn^{II} in compound **3**, each Cd^{II} atom is connected to four neighbouring Cd^{II} ions through four ligand molecules to form rhombohedral grids with diagonal distances of Cd···Cd 16.794(52) Å and 22.573(2) Å, respectively (Fig. S31†). These grids extend within the *bc*-plane thus forming a 2-D polymer of Cd^{II} with a (***4,4***)-net topology (Fig. 3b and c). The *tolyl*-fragments of the tosylate anions are oriented into the cavity of the tetranuclear Cd_4L_4-frames and occupy the space together with DCM molecules. The latter are bound by short contacts to oxygen atoms of the tosylate anions (H···O contact distances = 2.525(1) Å, Fig. 3c, S29†). At the same time, DCM molecules form Cl···π interactions with the anthracene linkers at a distance of Cl(1)–C$_{(centr.)}$ = 3.340(9) Å (Fig. 3c, Fig. S29†). The assembly of the 2-D layers along the *a*-direction leads to the formation of a 3-D polymer, where 1-D channels encapsulate the tosylate anions and DCM molecules (Fig. 3d).

{[Cd(μ$_2$-L)$_2$(*p*-Tos)$_2$]·2(MeOH)·1(Dioxane)}$_n$ (5). **5** crystallizes in the monoclinic space group $P2_1/n$ and shows a structure closely related to **4**. In this compound, the ligand molecules show the *cis*-conformation with interplanar angles between imidazole and anthracene of 83.2(2)° and 87.78(2)° (Fig. 4a, S33†). As a comparison, it is important to remember that the ligand molecules adopted the *trans*-conformation in compound **4**. Cd^{II} ions in compound **5** have pseudo-octahedral coordination geometries formed by four nitrogen atoms of **L** [Cd(1)–N(1) = 2.336(2) Å and Cd(1)–(N2) = 2.318(2) Å] in equatorial positions, while the axial positions are occupied by two oxygen atoms from tosylate anions [Cd(1)–O(1) = 2.290(2) Å] (Fig. 4a). The coordination angles around Cd^{II} ions are between N(1)–Cd(1)–O(1) = 87.94(13)° and N(2)–Cd(1)–(O1) = 91.78(14)° (Table 2). Ligands in *cis*-conformation connect Cd^{II} ions in characteristic rhombohedral grids with diagonal Cd···Cd distances of 13.388 Å and 23.816 Å, respectively (Fig. S34†). As for compound **4**, compound **5** shows an extended structure built on rhombohedral grids of Cd^{II} within the *ab*-plane, resulting in the creation of a 2-D supramolecular coordination polymer with a (***4,4***) topology of the net (Fig. 4b). The *tolyl*-groups of the tosylate anions logged in the cavity of the grid, thus occupying the available space. However, the *tolyl*-fragments show a positional disorder due to their free

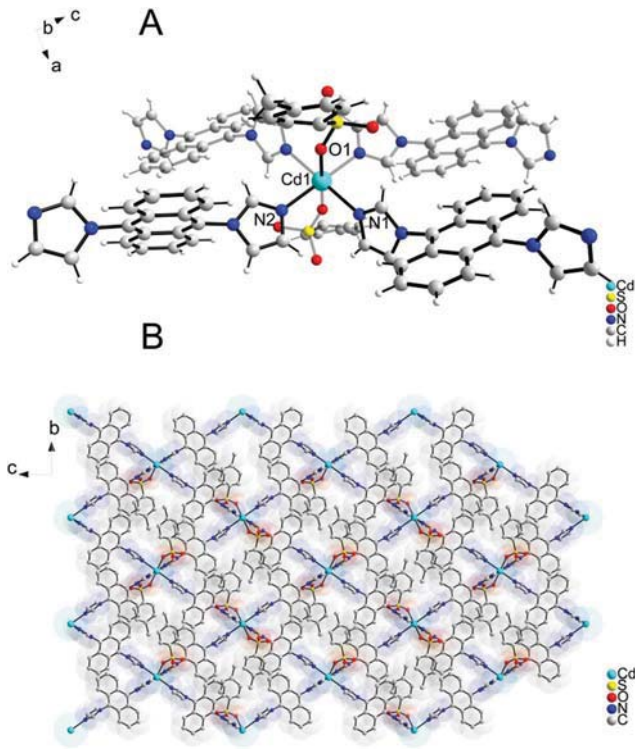

Fig. 4 Crystal structure of compound **5**: (A) coordination unit of {[Zn(μ$_2$-L)$_2$(*p*-Tos)$_2$]·2MeOH·2Dioxane}$_n$; (B) formation of the characteristic 2-D coordination polymer structure with topology of the nets – *4,4*.

rotation inside the cavity (Fig. S34 and S35†). The methanol molecules occupy the space in between the 2-D lattices and are oriented by hydrogen bonding with the tosylate anions (H(4)$_{MeOH}$–O(3)$_{tos.}$ = 2.080(2) Å and O(4)$_{MeOH}$–H(4)–O(3)$_{tos.}$ = 170.21°, Fig. S36†). Four dioxane molecules fill the rest of the cavity (Fig. S36 and S37†). The 2-D (***4,4***)-lattices based on **L** and Cd^{II} are weakly interconnected by short contacts between the imidazole proton and the tosylate oxygen atom with a distance of H(3)$_{imidazole}$–O(3)$_{tos.}$ = 2.585(2) Å. The extended structure might be described as the connection of 2-D coordination ***4,4***-nets to a 3-D supramolecular polymer of Cd^{II}. In addition, compound **5** should be considered as a structural isomer of compound **4**.

{[Zn(μ$_2$-L)$_2$(CF$_3$CO$_2$)$_2$]·2(Dioxane)}$_n$ (6). Compound **6** crystallizes in the monoclinic space group $P2_1/n$. The Zn^{II} ions show a distorted pseudo-octahedral coordination geometry. Four **L** molecules occupy *via* N atoms the equatorial positions with non-equivalent distances of Zn(1)–N(1) = 2.111(4) Å and Zn(1)–N(2) = 2.154(4) Å (Table 2). The axial positions are occupied by the O-atoms from the $CF_3CO_2^-$ anions at distances of Zn(1)–O(1) = 2.167(3) Å, and Zn(1)–O(2) = 2.197(4) Å. The coordination angles around Zn^{II} deviate from the ideal one with parameters of O(1)–Zn(1)–N(1) = 84.52(15)° and O(1)–Zn(1)–N(2) = 90.61(16)° (Fig. 5a). In contrast to compounds **1–5**, the Zn^{II} ions in **6** are connected through four bridging ligand molecules of different conformations, two of which with a *cis*- and two with a *trans*-conformation. The interplanar angles between

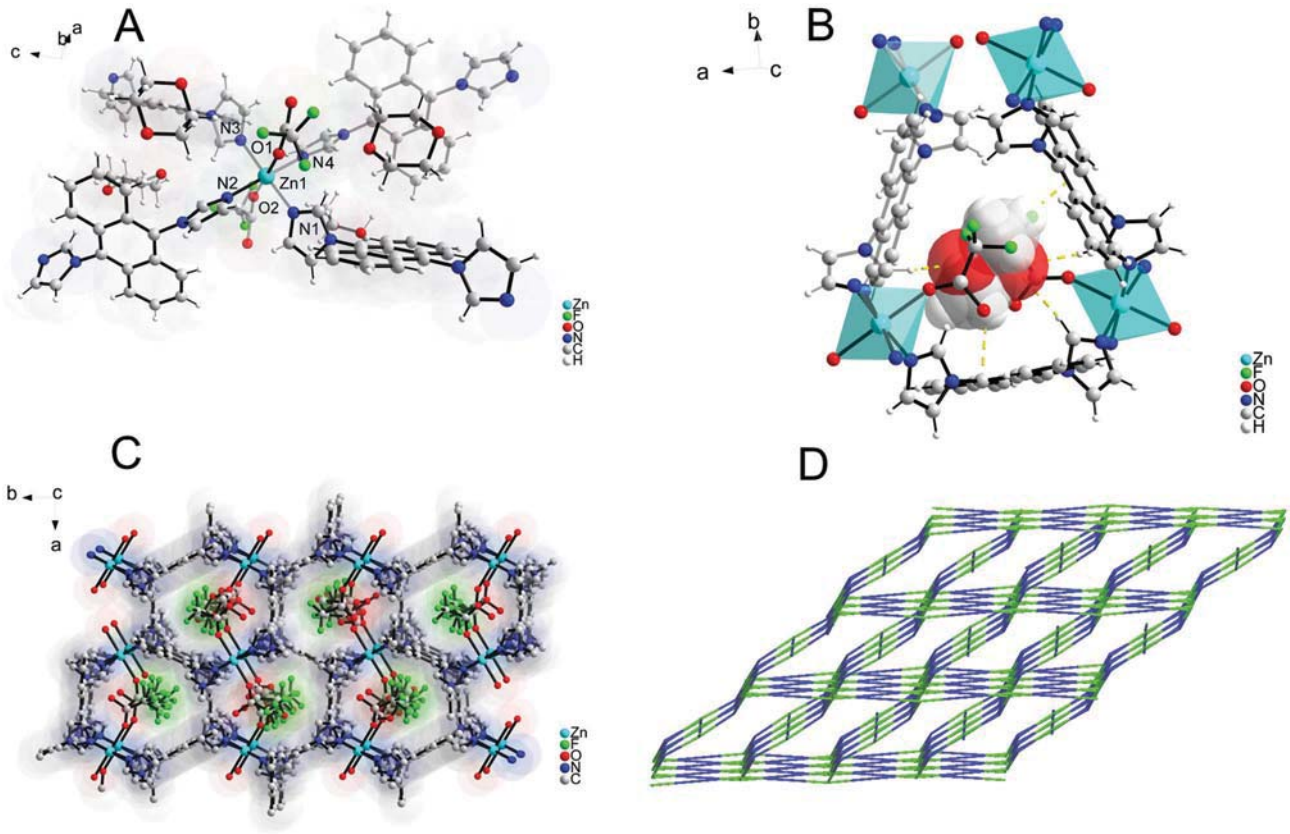

Fig. 5 Crystal structure of compound $\{[Zn(\mu_2\text{-}L)_2(CF_3CO_2)_2]\cdot 2(Dioxane)\}_n$ **6**: (A) representation of the coordination unit of compound **6** with bond distances [Zn(1)–N(1) = 2.111(4) Å Zn(1)–N(2) = 2.154(4) Å] and [Zn(1)–O(1) = 2.167(3) Å, Zn(1)–O(2) = 2.197(4) Å]; (B) formation of the cavity by three moieties of anthracene from **L** due to the coordination to Zn^{II} where a guest molecule of dioxane is trapped by the formation of intermolecular short van der Waals contacts; (C) the 3-D structure of the coordination framework of compound **6** showing closed channels filled with dioxane and closed by $CF_3CO_2^-$ anions; (D) simplified framework of the 3-D polymer **6** with topological type $CdSO_4$ with symbols for framework ***cds***.

the imidazole groups and the anthracene moiety amount to 75.73° for the *cis*- and 87.6° for the *trans*-isomer (Fig. S40†). Fig. 5d shows the 2-D lattice in compound **6**, where bent blue linkers represent *cis*-**L**, and straight blue ones refer to the *trans*-conformation. Green linkers indicate the Zn^{II} coordination nodes in **6**. With this alternation of *cis*- and *trans*-**L** for coordinating Zn^{II} ions, a new 3-D framework is formed with the ***cds*** topology of a 3-nodal net as determined using TOPOS software[29] (Fig. 5c and d). Voids in the 3-D framework are filled with molecules of dioxane, which are trapped in the cavity formed by three linkers of **L** (Fig. 5b). These anthracene supramolecular cavities constituted one molecule of **L** in *trans*- and two molecules of **L** in *cis*-conformation. The top and bottom of this cavity is "closed" by two $CF_3CO_2^-$ anions. The general structure of the compound can be described as a 3-D supramolecular framework with the ***cds*** topology and encapsulated dioxane molecules.

Crystal structure comparison

The crystallographic study of compounds **1–6** shows that they share common structural building blocks, based on the formation of 2-D ***4,4***-topological nets. However, compound **6** shows simultaneously two different conformations of **L**, which leads to the formation a 3-D framework instead of 2-D nets. Coordination polymers with non-coordinating anions of *Td* symmetry **1** and **2** feature a pseudo-tetrahedral coordination geometry around the metal ions, whereas compounds **3–6** with tosylate or TFA anions show preferentially distorted pseudo-octahedral geometries around the metal ions leading to the establishment of a 3-D supramolecular assembly of 2-D polymers. The anions hence seem to play a role as a predefining template in the formation of the coordination polyhedron in the obtained structures.[30] The ligand **L** adopts different *cis*- and *trans*-conformations with respect to the two imidazole groups and serves as a bidentate bridging linker. The change of conformation presumably occurs during solvation processes of **L**, which take place in the presence of polar solvent mixtures MeOH–dioxane (1 : 1) and MeOH–DCM (4 : 1) due to the low activation energy of the C–N bond in which **L** was found by DFT calculations (Fig. S56 and 57†). Compounds **1**, **2** and **5** adopt preferentially in their structure a *cis*-conformation of **L**, whereas structures **3** and **4** indicate the presence of *trans*-isomers which are formed in a relatively less polar solvent system 1 : 4 of MeOH–DCM. The conformations of the ligand have also an influence on the formation of the extended structure of the coordination polymers. 2-D polymers were formed with the ***4,4***-net topology for compounds **1–5**, but a mixed con-

formation system results in the ***cds*** topology for compound **6**. Related **L**-based coordination polymers with Cd^{II}, Co^{II}, and Ni^{II} were previously reported (Table 3).[23–26] Most of the reported CPs show *trans*-**L**, and only one example of Cd^{II} has been reported with a mixed ligand system where **L** adopts *cis*-conformation [Cd(*Hbtc*)(*cis*-**L**)]·3(H_2O).[23] This complex was obtained from water solution at 140 °C under hydrothermal conditions, in which **L** might be quite flexible with respect to the change of conformation. However, due to the limited solubility of **L** in H_2O–organic solvent systems, a complete dissolution of **L** may not take place, a situation which may explain the scarce reports of complexes with *trans*-**L** conformation.[23–26] Based on the obtained results and analyzed structures of **L**, it seems that not only the polarity of the solvent(s) determines the *cis* or *trans* arrangement of **L**, but also nature of the metal ion and the counter ion contribute to the configuration of **L**. The relative stiffness of **L** based on the central rigid anthracene moiety implies that the ligand acts as a bridging rather than a chelating ligand, which leads to the formation of polymeric structures with Zn^{II} and Cd^{II} rather than of molecular complexes.

Thermal stability

Thermogravimetric analyses of **1–6** were performed under an N_2 atmosphere from 25 to 600 °C with a heating rate of 1 °C min^{-1}. The corresponding TGA curves are shown in Fig. S43–S47.† Complex **1** shows the solvent evaporation of DCM and MeOH at room temperature while exposed to air, a slight weight loss of ~5.35% before 320 °C corresponds to the removal of ~2 MeOH molecules. Further heating over 320 °C leads to the decomposition of the coordination polymer. A similar behaviour was observed for complex **2** under heating from 25 to 100 °C with an observed mass loss of ~5%, which was also assigned to two molecules of MeOH. The full decomposition was observed above 320 °C. Complexes **3** and **4** show a mass loss of ~5.5% and ~3% in the 25–60 °C range, which corresponds to ~2(MeOH) molecules for **3** and ~0.5 (DCM) molecules for **4**. Heating over 280 °C leads to a stepwise mass loss followed by the decomposition of the organic ligand and anion. **5** shows below 260 °C a one-step mass loss of ~8% at ~110 °C corresponding to the removal of approximately one molecule of dioxane. Heating over 260 °C shows a multi-step decomposition of 2-D nets of **5**. The thermal stability of **6** reveals that the complex is not stable towards heating from 25 to 110 °C with a total mass loss of ~38% corresponding to the removal of four molecules of dioxane. Heating over 220 °C leads to a slow one-step decomposition of the complex. Ultimately, complexes **1–2** with ClO_4^- and BF_4^- show the highest thermal stability in comparison with **3–5** which have tosylate as the anion. Compound **6** shows the lowest thermal stability among all isolated complexes due to the presence of pores, which contain encapsulated solvent molecules that enhance the collapsing of the framework at lower temperature.

Emission and absorption properties§

The synthesis of coordination polymers with conjugated organic linkers between the transition metals is a promising approach for obtaining new functional luminescent materials, especially for the systems with d^{10} or d^{10}–d^{10} transitions.[20] In the present work, we studied the luminescence behaviour of complexes **1–6** in the solid state at room temperature. The emission and absorption bands were observed for **L** and **1–6**, and are presented in Fig. 6. Based on the absorption of the ligand and compounds **1–6**, all complexes were excited at 375 ± 2 nm, and the emission bands are observed in the 430–600 nm wavelength range. These bands can be assigned to intra-ligand (n–π* and π–π*)-electronic transitions as they

Table 3 Coordination polymers reported with L in different conformations

	Compound	L	Solvent system	Yield, %
1	[Cd(oba)(**L**)$_{0.5}$][23]	*Trans*	H_2O-140 °C	50
2	[Cd(Hbtc)(**L**)]·3(H_2O)[23]	*Cis*	H_2O-140 °C	43
3	[Cd_3(2-stp)$_2$(**L**)$_6$(H_2O)$_2$][23]	*Trans*	H_2O-140 °C	42
4	[Co_3(2-stp)$_2$(**L**)$_6$(H_2O)$_2$][23]	*Trans*	H_2O-140 °C	44
5	[Ni_3(2-stp)$_2$(**L**)$_6$(H_2O)$_2$][23]	*Trans*	H_2O-140 °C	53
6	[Co(L)$_2$(NO_3)$_2$·2(CH_2Cl_2)][24]	*Trans*	MeOH–DCM	64
7	[Co(**L**)$_{2.5}$(NO_3)$_2$·H_2O][24]	*Trans*	H_2O-110 °C	54
8	[Co(bdc)(**L**)(H_2O)·Co(bdc)(**L**)$_2$·(H_2O)][24]	*Trans*	H_2O-170 °C	46
9	[Cd(bdc)(**L**)$_{0.5}$(MeOH)]·(DMA)$_{0.5}$[25]	*Trans*	MeOH–DMA-100 °C	51
10	[Cd_2O(*1,4*-ndc)$_2$(**L**)$_2$(H_2O)]·DMA[25]	*Trans*	H_2O–DMA-100 °C	66
11	[Cd(*1,4*-ndc)(L)]·MeOH[25]	*Trans*	MeOH–DMA-100 °C	62
12	[Cd(dpdc)(L)$_{0.5}$]·DMF[25]	*Trans*	MeOH–DMF-H_2O-100 °C	58
13	[Cd(dpdc)(L)]·DEF[25]	*Trans*	DEF-100 °C	78
14	[Ni(oba)(L)$_{1.5}$(H_2O)][26]	*Trans*	H_2O-140 °C	75
15	[Ni(Hsip)(L)$_{1.5}$(H_2O)][26]	*Trans*	H_2O-140 °C	81
16	{[Zn(μ_2-L)$_2$](ClO_4)$_2$·2(MeOH)·2(DCM)}$_n$ (**1**)[a]	*Cis*	MeOH–DCM[b] (4 : 1)	68
17	{[Zn(μ_2-L)$_2$](BF_4)$_2$·2(MeOH)·2(DCM)}$_n$ (**2**)[a]	*Cis*	MeOH–DCM[b] (4 : 1)	60
18	{[Zn(μ_2-L)$_2$(*p*-Tos)$_2$]·2(DCM)·2(MeOH)}$_n$ (**3**)[a]	*Trans*	MeOH–DCM[b] (1 : 4)	52
19	{[Cd(μ_2-L)$_2$(*p*-Tos)$_2$]·2(DCM)}$_n$ (**4**)[a]	*Trans*	MeOH–DCM[b] (1 : 4)	79
20	{[Cd(μ_2-L)$_2$(*p*-Tos)$_2$]·2(MeOH)·1(Dioxane)}$_n$ (**5**)[a]	*Cis*	MeOH–dioxane[b] (1 : 1)	83
21	{[Zn(μ_2-L)$_2$(CF_3CO_2)$_2$]·2(Dioxane)}$_n$ (**6**)[a]	*cis & trans*	MeOH–dioxane[b]	95

[a] Reported in this work. [b] Room temperature.

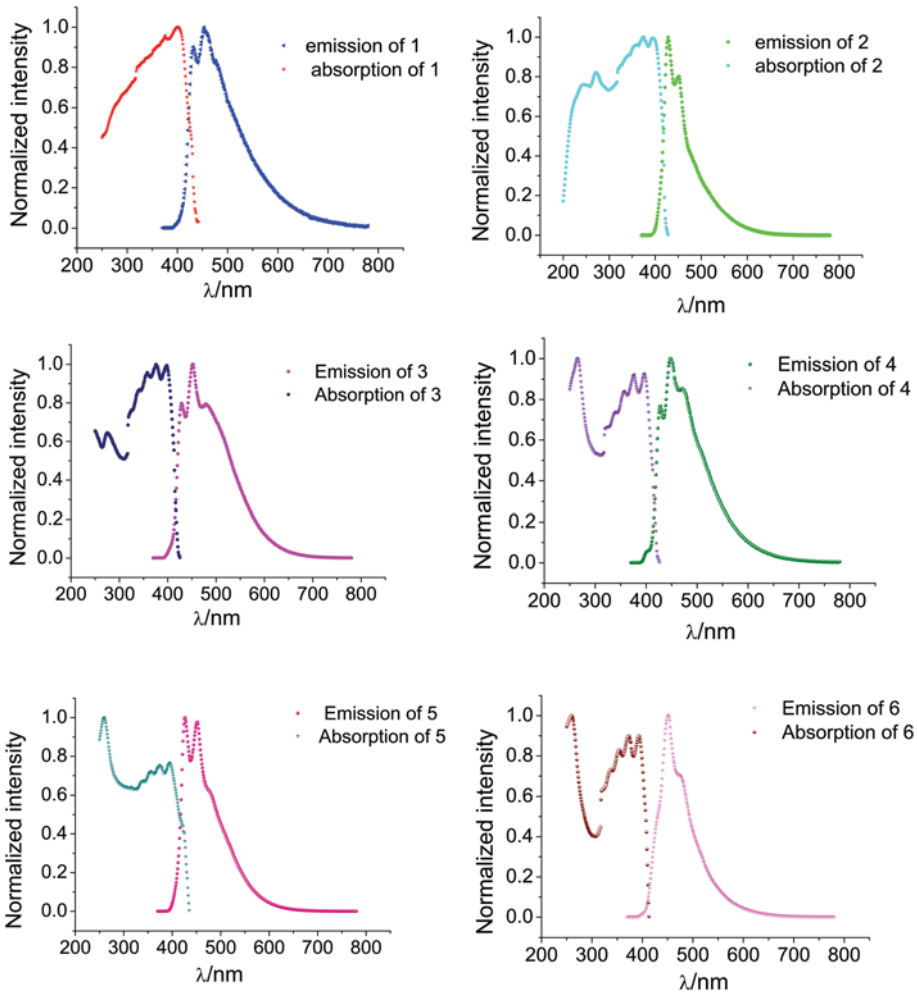

Fig. 6 Solid-state UV-Vis and PL spectra of obtained compounds **1–6** measured at rt excited at 350 nm.

correspond well with the observed emissions of the free ligand **L** (Fig. S49 and S50†).[21,22]

According to Fig. 6, all the emission and absorption spectra are similar and display standard L(π*–π) transitions with more or less resolved vibronic structures.

In order to investigate the lifetime of the luminescence properties of the complexes, the compounds in the solid state were excited with a *EPL pulsed diode laser* (Edinburg Instruments) system, using optical fibres with a time delay of the shutter 50 ns. Most of the obtained complexes show a biexponential decay character of the emission curves with t_1 and t_2 equal for all complexes and are in the range of 5–7 ns (Fig. S52 and 53†).

The Quantum yields (QYs) of the obtained compounds were determined in the solid state using an integrating sphere at room temperature. A value of 28% was measured for **L** while low quantum yield values of 0.07% and 0.02% were determined for complexes **1** and **2** respectively in the presence and absence of crystallization solvent molecules. The QYs were found to be of the same order as for the solvent-containing ones. In complexes **3–5** that include *p*-Tos as the anion for Zn^{II} and Cd^{II}, a higher intensity of luminescence was observed with quantum yield values of 4% for **3**, 9% for **4** and 12% for **5**. The complex **6** possessing ligands in different *trans*- and *cis*-conformations has been characterized to possess an average quantum efficiency of 9%. Nevertheless, all complexes show lower quantum yields than the free **L** which can therefore be tentatively explained by the presence of intermolecular interactions with guest solvent molecules in the crystal packing of structures **1–6**. A recent report by Celestino and Eisfeld[31] might explain our short lifetimes of fluorescence. The extended packing of J-aggregates reduces the lifetime by a factor of $1/N$ where N is the number of packed monomers. For the extended H-packing, no emission should occur as only dark states at the bottom are occupied. This phenomenon of quenching of the entire luminescence could be used for the sensing of solvent molecules by inducing further J-aggregation. Overall, the obtained Cd^{II}-based complexes **4** and **5** have a higher QY efficiency compared to the Zn^{II} complexes.

Sensing of nitro explosives. Complex **6** was chosen for sensing tests as it has sufficiently large pores that can be exchanged with analytes. As a standard procedure complex **6**

was dried under vacuum for 1 h upon heating at 50 °C, and then the tube was filled with an inert gas. 1 mg of complex was placed in the quartz cuvette and filled with 2 mL of dry acetonitrile. The addition of a nitro compound was achieved from a 1 mM stock solution, and the spectra were collected from 400–700 nm upon excitation at 405 nm. Fluorescent sensing titrations were performed with traces of: nitrobenzene, *o*-dinitrobenzene, 4,6-dinitropyrogallol, *p*-bromonitrobenzene, *m*-chloro-nitrobenzene, chloro-2,4-dinitrobenzene, 2,4-dinitrophenol, and *o*-nitrophenol are shown in Fig. 7. Larger shifts are observed for bis-substituted nitro compounds and they show a response for luminescence with a blue-shift (see ESI Fig. S58,† Fig. 7). In particular, 4,6-dinitropyrogallol reaches a maximum with a luminescence shift of **6** by *ca.* 50 nm. The second nitro compound, 2,4-dinitrophenol, leads simultaneously to the shift and quenching of luminescence of **6**. Mono-substituted compounds thus show a less sensitive response and have a weaker impact on the shift of the luminescence of **6**.

DFT calculations. To understand a possible influence of solvent molecules on the conformation of **L**, we performed DFT calculations with the B3LYP/6-31G* basis set using SPARTAN software package.[27] It revealed that the *trans*-isomer is more stable under *vacuum* than the *cis*-isomer, by 0.41 eV. Interestingly, the situation changes when dissolved in polar MeOH–dioxane or MeOH–DCM The solvation energy of *cis*-**L** is lower than that of *trans*-**L** by 1.32 kJ mol^{-1}. *trans*-**L** has a $\Delta E_{(LUMO-HOMO)}$= 3.46 eV (Fig. S53†) which correlates well with that of the absorption bands with a maximum calculated at 358 nm. However, the *cis*-**L** energy gap is shifted to lower energies of $\Delta E_{(LUMO-HOMO)}$ = 2.94 eV (Fig. S54†) with a calculated maximum at 421 nm. Hence, the *cis*-conformer is preferred in most of the solvents due to lower solvation energies. Nevertheless, a relatively small activation energy of 0.82 eV (19.7 kJ mol^{-1}, Fig. S56 and 57†) to pass from the *trans*- to the *cis*-isomer gives rise to the formation of a mixed system **6** as well as different coordination polymers with **L** in either conformation in **1–5**.

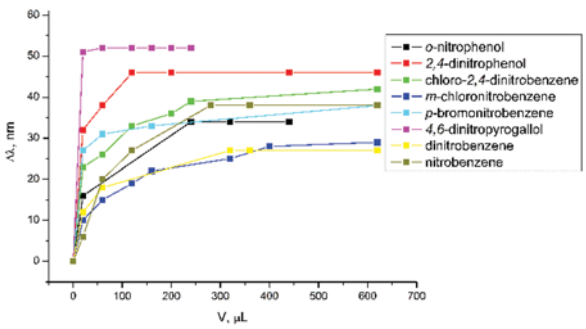

Fig. 7 Sensing experiments of nitro-compounds with complex **6**. The plot shows the shift of luminescence maxima of **6** for different concentration of the added nitro compound.

Conclusions

In summary, we report here an Ullmann-type "Cu-free" synthesis of the 9,10-di(1*H*-imidazol-1-yl)-anthracene ligand **L**, which was used for preparing six new coordination polymers of Zn^{II} and Cd^{II}. **L** adopts different conformations: *cis*- or *trans*- of the functional groups, due to rotation around the C–N bond which occurs in polar organic solvents. Both isomers are present in the single crystal structures of complexes **1–6**. The structures of compounds **1–5** revealed the self-assembly of 2D coordination polymers with a ***4,4***-topology of the nets, while complex **6** crystalizes with a ***cds*** topology of a 3-D framework. Solvent guest molecules get encapsulated in the voids between layers. The fluorescence spectra show that these complexes have a strong blue emission in the 400–600 nm wavelength range. These emissions may be assigned to intra-ligand (n–π* or π–π*) electronic transitions. This makes them potential candidates for applications in light emitting devices and luminescent sensors for nitro explosives.

Conflicts of interest

There are no conflicts to declare.

Acknowledgements

We would like to acknowledge the Swiss National Science Foundation SNSF, and the NCCR "Bioinspired Materials" as well as the Fribourg Centre for Nanomaterials for the support and opportunity to work under this project. KR acknowledges the Swiss National Science Foundation for an EPM fellowship. Thanks to Dr Aurélien Crochet for the help with X-Ray diffraction methods.

Notes and references

1 (*a*) H. Xu, R. Chen, Q. Sun, W. Lai, Q. Su, W. Huang and X. Liu, *Chem. Soc. Rev.*, 2014, **43**, 3259; (*b*) J. Heine and K. Müller-Buschbaum, *Chem. Soc. Rev.*, 2013, **42**, 9232.
2 (*a*) Y. Wei, H. Dong, C. Wei, W. Zhang, Y. Yan and Y. Zhao, *Adv. Mater.*, 2016, **28**, 7424; (*b*) L. R. Mingabudinova, V. V. Vinogradov, V. A. Milichko, E. Hey-Hawkins and A. V. Vinogradov, *Chem. Soc. Rev.*, 2016, **45**, 5408; (*c*) F.-Y. Yi, D. Chen, M.-K. Wu, L. Han and H.-L. Jiang, *ChemPlusChem*, 2016, **81**, 675.
3 (*a*) Z. Hu, B. Deibert and J. Li, *Chem. Soc. Rev.*, 2014, **43**, 5815; (*b*) Y. Cui, B. Chen and G. Qian, *Coord. Chem. Rev.*, 2014, **273**, 76.
4 K. Wang, T. Liu, Y. Liu, X. Tian, J. Sun and Q. Zhang, *CrystEngComm*, 2016, **18**, 8301.
5 (*a*) E. Coronado and G. Espallargas, *Chem. Soc. Rev.*, 2013, **42**, 1525; (*b*) R. Ricco, L. Malfatti, M. Takahashi, A. Hill and P. Falcaro, *J. Mater. Chem. A*, 2013, **1**, 13033.
6 J.-R. Li, R. Kuppler and H.-C. Zhou, *Chem. Soc. Rev.*, 2009, **38**, 1477.

7 M. Ranocchiari and J. Bokhoven, *Phys. Chem. Chem. Phys.*, 2011, **13**, 6388.

8 (*a*) N. Stock and S. Biswas, *Chem. Rev.*, 2012, **112**(2), 933; (*b*) M. Zhang, M. Bosch, T. Gentle and H.-C. Zhou, *CrystEngComm*, 2014, **16**, 4069; (*c*) P. Sontz, J. Bailey, S. Ahn and F. Tezcan, *J. Am. Chem. Soc.*, 2015, **137**, 11598; (*d*) L. Basabe-Desmonts, D. Reinhoudt and M. Crego-Calama, *Chem. Soc. Rev.*, 2007, **36**, 993; (*e*) O. Farha and J. Hupp, *Acc. Chem. Res.*, 2010, **43**(8), 1166; (*f*) Y. Xie, Z. Yu, X. Huang, Z. Wang, L. Niu, M. Teng and J. Li, *Chem. – Eur. J.*, 2007, **13**, 9399; (*g*) T. Cook, Y.-R. Zheng and P. Stang, *Chem. Rev.*, 2013, **113**(1), 734.

9 G. Desiraju, *Angew. Chem., Int. Ed. Engl.*, 1995, **34**, 2311.

10 (*a*) H. Quah, W. Chen, M. Schreyer, H. Yang, M. Wong, W. Ji and J. Vittal, *Nat. Commun.*, 2015, **6**, 7954; (*b*) P. Mahato, A. Monguzzi, N. Yanai, T. Yamada and N. Kimizuka, *Nat. Mater.*, 2015, **14**, 924; (*c*) C. Y. Lee, O. K. Farha, B. J. Hong, A. A. Sarjeant, S. T. Nguyen and J. T. Hupp, *J. Am. Chem. Soc.*, 2011, **133**, 15858; (*d*) X. Zhang, B. Li, H. Ma, L. Zhang and H. Zhao, *Appl. Mater. Interfaces*, 2016, **8**, 17389; (*e*) N. Yanai and N. Kimizuka, *Chem. Commun.*, 2016, **52**, 5354; (*f*) J. Chen, A. Neels and K. M. Fromm, *Chem. Commun.*, 2010, **46**, 8282.

11 X.-L. Yang, X. Chen, G.-H. Hou, R.-F. Guan, R. Shao and M.-H. Xie, *Adv. Funct. Mater.*, 2016, **26**, 393.

12 J. Drewrya and P. Gunning, *Coord. Chem. Rev.*, 2011, **255**, 459.

13 J. Morris, M. Mahaney and J. Huber, *J. Phys. Chem.*, 1976, **80**, 969.

14 (*a*) S.-S. Chen, *CrystEngComm*, 2016, **18**, 6543; (*b*) M. Eddaoudi, D. F. Sava, J. F. Eubank, K. Adil and K. Guillerm, *Chem. Soc. Rev.*, 2015, **44**, 228; (*c*) Z.-G. Gu, Y.-T. Liu, X.-J. Hong, Q.-G. Zhan, Z.-P. Zheng, S.-R. Zheng, W.-S. Li, S.-J. Hu and Y.-P. Cai, *Cryst. Growth Des.*, 2012, **12**, 2178; (*d*) F. Wang, X. Ke, J. Zhao, K. Deng, X. Leng, Z. Tian, L. Wen and D. Li, *Dalton Trans.*, 2011, **40**, 11856.

15 (*a*) P. Grondin, D. Siretanu, O. Roubeau, M.-F. Achard and R. Clerac, *Inorg. Chem.*, 2012, **51**, 5417; (*b*) F. Ullmann, *Eur. J. Inorg. Chem.*, 1903, **36**, 2382.

16 G. M. Sheldrick, *Acta Crystallogr., Sect. A: Found. Adv.*, 2015, **71**, 3.

17 (*a*) F. R. Ahmed, *Crystallographic Computing*, Munksgaard, Copenhagen, 1970, p. 255; (*b*) *Stoe & Cie., X-AREA, X-RED, X-RED32, X-SHAPE*, Darmstadt, Germany, 2002.

18 (*a*) S. Holmes, S. Mckinley and G. Girolami, *Inorg. Synth.*, 2002, **33**, 91; (*b*) M. Suresh, S. A. Bahadur and S. Athimoolam, *J. Mater. Sci.*, 2016, **27**, 4578.

19 W. E. Brittin, *J. Chem. Educ.*, 1945, **22**, 145.

20 (*a*) X. Li and H. Patterson, *Materials*, 2013, **6**, 2595; (*b*) X.-m. Liu, X.-y. Mu, H. Xia, L. Ye, W. Gao, H.-y. Wang and Y. Mu, *Eur. J. Inorg. Chem.*, 2006, **21**, 4317; (*c*) V. Yam and K. Wong, *Chem. Commun.*, 2011, **47**, 11579.

21 (*a*) Y. Zou, J. Chen, Y.-Y. Li, L. Li, J.-L. Liu and X.-M. Ren, *RSC Adv.*, 2015, **5**, 78642; (*b*) Y. Tao, J.-R. Li, Q. Yu, W.-C. Song, X.-L. Tong and X.-H. Bu, *CrystEngComm*, 2008, **10**, 699.

22 (*a*) J. Dai, X. Wu, Z. Fu, C. Cui, S. Wu, W. Du, L. Wu, H. Zhang and Q. Sun, *Inorg. Chem.*, 2002, **41**, 1391.

23 C.-H. Ke, G.-R. Lin, B.-C. Kuo and H. M. Lee, *Cryst. Growth Des.*, 2012, **12**, 3758.

24 H.-J. Lee, P.-Y. Cheng, C.-Y. Chen, J.-S. Shen, D. Nandi and H. M. Lee, *CrystEngComm*, 2011, **13**, 4814.

25 X. Li, L. Yang, L. Zhao, X.-L. Wang, K.-Z. Shao and Z.-M. Su*, *Cryst. Growth Des.*, 2016, **16**, 4374.

26 C.-H. Kea and H. M. Lee, *CrystEngComm*, 2012, **14**, 4157.

27 *Spartan'08*, Wavefunction, Inc., Irvine, CA; Y. Shao, L. F. Molnar, Y. Jung, J. Kussmann, C. Ochsenfeld, S. T. Brown, A. T. B. Gilbert, L. V. Slipchenko, S. V. Levchenko, D. P. O'Neill, R. A. DiStasio Jr., R. C. Lochan, T. Wang, G. J. O. Beran, N. A. Besley, J. M. Herbert, C. Y. Lin, T. Van Voorhis, S. H. Chien, A. Sodt, R. P. Steele, V. A. Rassolov, P. E. Maslen, P. P. Korambath, R. D. Adamson, B. Austin, J. Baker, E. F. C. Byrd, H. Dachsel, R. J. Doerksen, A. Dreuw, B. D. Dunietz, A. D. Dutoi, T. R. Furlani, S. R. Gwaltney, A. Heyden, S. Hirata, C.-P. Hsu, G. Kedziora, R. Z. Khalliulin, P. Klunzinger, A. M. Lee, M. S. Lee, W. Z. Liang, I. Lotan, N. Nair, B. Peters, E. I. Proynov, P. A. Pieniazek, Y. M. Rhee, J. Ritchie, E. Rosta, C. D. Sherrill, A. C. Simmonett, J. E. Subotnik, H. L. Woodcock III, W. Zhang, A. T. Bell, A. K. Chakraborty, D. M. Chipman, F. J. Keil, A. Warshel, W. J. Hehre, H. F. Schaefer, J. Kong, A. I. Krylov, P. M. W. Gill and M. Head-Gordon, *Phys. Chem. Chem. Phys.*, 2006, **8**, 3172.

28 PLATON, A. L. Spek, *Acta Crystallogr., Sect. D: Biol. Crystallogr.*, 2009, **65**, 148–155.

29 (*a*) TOPOS, V. A. Blatov, *TOPOS*, Samara State University, Russia, 2004; (*b*) V. A. Blatov, A. P. Shevchenko and V. N. Serezhkin, *J. Appl. Crystallogr.*, 2000, **33**, 1193.

30 N. Gimeno and R. Vilar, *Coord. Chem. Rev.*, 2006, **250**, 3161.

31 A. Celestino and A. Eisfeld, *J. Phys. Chem. A*, 2017, **121**, 5948.